

Spectral Anisotropy of Elsässer Variables in Two Dimensional Wave-vector Space as Observed in the Fast Solar Wind Turbulence

Limei Yan¹, Jiansen He¹, Lei Zhang¹, Chuanyi Tu¹, Eckart Marsch², Christopher H.K. Chen³, Xin Wang¹, Linghua Wang¹, Robert T. Wicks⁴

ABSTRACT

Intensive studies have been conducted to understand the anisotropy of solar wind turbulence. However, the anisotropy of Elsässer variables (\mathbf{Z}^\pm) in 2D wave-vector space has yet to be investigated. Here we first verify the transformation based on the projection-slice theorem between the power spectral density $\text{PSD}_{2\text{D}}(k_\parallel, k_\perp)$ and the spatial correlation function $\text{CF}_{2\text{D}}(r_\parallel, r_\perp)$. Based on the application of the transformation to the magnetic field and the particle measurements from the WIND spacecraft, we investigate the spectral anisotropy of Elsässer variables (\mathbf{Z}^\pm), and the distribution of residual energy E_R , Alfvén ratio R_A and Elsässer ratio R_E in the (k_\parallel, k_\perp) space. The spectra $\text{PSD}_{2\text{D}}(k_\parallel, k_\perp)$ of \mathbf{B} , \mathbf{V} , and $\mathbf{Z}_{\text{major}}$ (the larger of \mathbf{Z}^\pm) show a similar pattern that $\text{PSD}_{2\text{D}}(k_\parallel, k_\perp)$ is mainly distributed along a ridge inclined toward the k_\perp axis. This is probably the signature of the oblique Alfvénic fluctuations propagating outwardly. Unlike those of \mathbf{B} , \mathbf{V} , and $\mathbf{Z}_{\text{major}}$, the spectrum $\text{PSD}_{2\text{D}}(k_\parallel, k_\perp)$ of $\mathbf{Z}_{\text{minor}}$ is distributed mainly along the k_\perp axis. Close to the k_\perp axis, $|E_R|$ becomes larger while R_A becomes smaller, suggesting that the dominance of magnetic energy over kinetic energy becomes more significant at small k_\parallel . R_E is larger at small k_\parallel , implying that $\text{PSD}_{2\text{D}}(k_\parallel, k_\perp)$ of $\mathbf{Z}_{\text{minor}}$ is more concentrated along the k_\perp direction as compared to that of $\mathbf{Z}_{\text{major}}$. The residual energy condensate at small k_\parallel is consistent with simulation results in which E_R is spontaneously generated by Alfvén wave interaction.

Subject headings: solar wind — turbulence — waves

1. Introduction

MHD turbulence in the solar wind is considered to be a cascade of energy over different scales caused by the nonlinear interaction between counterpropagating Alfvén waves, which has

¹School of Earth and Space Sciences, Peking University, 100871 Beijing, China, jshept@gmail.com

²Institute for Experimental and Applied Physics, Christian Albrechts University at Kiel, D-24118 Kiel, Germany

³Department of Physics, Imperial College London, London, SW7 2AZ, United Kingdom

⁴Department of Space and Climate Physics, University College London, Gower Street, London, UK

been studied in detail by asymptotic solution (Howes & Nielson, 2013) and numerical simulation (Nielson et al., 2013). The cascade is anisotropic with the cascading direction mainly perpendicular to the local mean magnetic field (e.g. Goldreich & Sridhar, 1995). When the oppositely directed Alfvén waves carry unequal energy, the turbulence is imbalanced. Imbalanced weak (Galtier et al., 2000; Lithwick & Goldreich, 2003) and strong (Lithwick et al., 2007) turbulence have been studied intensively. In some theoretical studies, the energy spectrum of the Elsässer variables ($\mathbf{Z}^\pm = \mathbf{V} \pm \mathbf{b}$, $\mathbf{b} = \frac{\mathbf{B}}{\sqrt{\mu_0 \rho}}$) \mathbf{E}^\pm have a same scaling with different amplitudes. The scaling is $E^+ \propto E^- \propto k_\perp^{-3/2}$ with the phenomenon of dynamic alignment (Perez & Boldyrev, 2009), while the scaling is $E^+ \propto E^- \propto k_\perp^{-5/3}$ without the phenomenon of dynamic alignment (Lithwick et al., 2007). In the solar wind, especially in fast streams, imbalanced turbulence is usually observed (one of \mathbf{Z}^\pm is dominating). We define the dominant mode as $\mathbf{Z}_{\text{major}}$ which is typically the Alfvén wave propagating outward from the sun, while the subdominant mode $\mathbf{Z}_{\text{minor}}$ is weak and complicated. The subdominant mode has been suggested to be inward propagating Alfvén wave at high frequency and compressive events at low frequency (e.g. Bruno et al., 1996), magnetic structures (Tu & Marsch, 1992, 1993).

Without temperature anisotropies and relative drifts, if the MHD turbulence is only composed of counterpropagating Alfvén waves with no nonlinear interaction, the residual energy $E_R = v^2 - b^2$ would be zero. However in the solar wind, outward propagating Alfvén waves are often observed, while inward propagating Alfvén waves are rarely observed. Besides, there are also many structures like tangential discontinuities in the solar wind which may contribute more to the magnetic disturbances than the velocity fluctuations. These factors would lead to the residual energy being nonzero. Residual energy is high at low frequency / small k from observations (e.g. Roberts et al., 1987; Bavassano et al., 1998; Wicks et al., 2011), however it remains unknown whether the residual energy is mainly distributed along k_\parallel or k_\perp . In the solar wind turbulence, the residual energy at small scales near the dissipation range is usually less than 0 (e.g. Belcher & Davis, 1971; Matthaeus & Goldstein, 1982; Boldyrev et al., 2012; Chen et al., 2013). This is also noted in simulations (e.g. Grappin et al., 1983; Müller & Grappin, 2005; Gogoberidze et al., 2012). As revealed from recent simulations, the residual energy is concentrated at small k_\parallel (Boldyrev & Perez, 2009; Wang et al., 2011). The distribution of the residual energy in the wave-vector space will allow us to compare with these simulation results.

The presence of a mean magnetic field may lead to spectral anisotropy of magnetohydrodynamic (MHD) turbulence (Shebalin et al., 1983). Goldreich & Sridhar (1995) investigated the anisotropy in a balanced strong MHD turbulence with vanishing cross-helicity, revealing a spectrum perpendicular to the magnetic field of $E(k_\perp) \sim k_\perp^{-5/3}$, a parallel spectrum $E(k_\parallel) \sim k_\parallel^{-2}$, and a scaling relation $k_\parallel \sim k_\perp^{2/3}$ based on the critical balance assumption, i.e., the linear wave periods are comparable to the nonlinear turnover timescales. The anisotropic power and scaling of magnetic field fluctuations in the inertial range of high-speed solar wind turbulence is first reported by Horbury et al. (2008), who introduced the method to estimate the scale-dependent local \vec{B}_0 . The reduced spectrum has an index near -2 when $\theta_{BV} \rightarrow 0$ and an index near $-5/3$ when $\theta_{BV} \rightarrow 90$ where θ_{BV} is the angle between the magnetic field and the flow. Podesta (2009) gave similar results

using magnetic field measurements from the STEREO. Luo & Wu (2010) and Chen et al. (2011) also got a similar conclusion for the magnetic structure function. When the second order structure function of the magnetic fluctuations is decomposed into the components perpendicular (δB_{\perp}^2) and parallel (δB_{\parallel}^2) to the mean field, both components show spectral index anisotropy between the ion and electron gyroscopes in the fast solar wind (Chen et al., 2010). At these small scales the spectral index of δB_{\perp}^2 is -2.6 at large angles and -3 or steeper at small angles. This kind of spectral anisotropy of solar wind turbulence in the inertial range is probably related to the intermittency (Wang et al., 2014). Wicks et al. (2011) studied the anisotropy of the Elsässer variables in fast solar wind based on the reduced spectrum, finding that the dominant Elsässer mode is isotropic at low frequencies but becomes increasingly anisotropic at higher frequencies while the subdominant mode is anisotropic throughout. This result suggests that the anisotropy of the subdominant mode may be stronger than the dominant mode.

The spectral anisotropy has been studied extensively based on the reduced spectrum, while the anisotropy in wave-vector space is relatively rarely studied. The K-filtering method has been applied to the Cluster observations to investigate the anisotropy in wave-vector space (e.g. Sahraoui et al., 2010; Narita et al., 2010). However, this method is sensitive only to a limited number of wave modes and the scales comparable to the inter-spacecraft distance (Horbury et al., 2012). Based on single spacecraft measurements, He et al. (2013) first constructed the normalized power spectral density (PSD) of magnetic field fluctuations (\mathbf{B}) in 2D wave-vector space. They found that the PSD of \mathbf{B} shows an anisotropic distribution, which is mainly characterized by a ridge distribution inclined more toward k_{\perp} as compared to k_{\parallel} . The spectral anisotropy of velocity and Elsässer variables in wave-vector space has not been previously investigated. We will study them in this paper using the method contributed by He et al. (2013). Moreover, we will investigate the distribution of residual energy $E_R = E_v - E_b$, Alfvén ratio $R_A = \frac{E_v}{E_b}$ and Elsässer ratio $R_E = \frac{E_{Z_{\text{minor}}}}{E_{Z_{\text{major}}}}$ in the wave-vector space.

2. Benchmark test of the conversion between CF_{2D} and PSD_{2D}

To test the conversion between CF_{2D} and PSD_{2D} based on the projection-slice theorem, we first assume a double Gaussian distribution, a strong parallel component and a weak perpendicular component, for CF_{2D} using the formula given below:

$$CF_{2D}(r_{\parallel}, r_{\perp}) = \exp\left(-\frac{r_{\parallel}^2}{2\sigma_{\parallel 1}^2}\right) \cdot \exp\left(-\frac{r_{\perp}^2}{2\sigma_{\perp 1}^2}\right) + 3 \cdot \exp\left(-\frac{r_{\parallel}^2}{2\sigma_{\parallel 2}^2}\right) \cdot \exp\left(-\frac{r_{\perp}^2}{2\sigma_{\perp 2}^2}\right) \quad (1)$$

Based on this assumption, there are three ways to obtain the $\text{PSD}_{2\text{D}}$. The first way is to get the $\text{PSD}_{2\text{D}}$ directly from the corresponding formula :

$$\begin{aligned} \text{PSD}_{2\text{D}}(k_{\parallel}, k_{\perp}) = & \sigma_{\parallel 1} \cdot \exp\left(-\frac{k_{\parallel}^2 \cdot \sigma_{\parallel 1}^2}{2}\right) \cdot \sigma_{\perp 1} \cdot \exp\left(-\frac{k_{\perp}^2 \cdot \sigma_{\perp 1}^2}{2}\right) \\ & + 3 \cdot \sigma_{\parallel 2} \cdot \exp\left(-\frac{k_{\parallel}^2 \cdot \sigma_{\parallel 2}^2}{2}\right) \cdot \sigma_{\perp 2} \cdot \exp\left(-\frac{k_{\perp}^2 \cdot \sigma_{\perp 2}^2}{2}\right) \end{aligned} \quad (2)$$

The second way is to do the transformation based on the projection-slice theorem. Firstly, we make the 1 dimensional integration (1D-INT) of $\text{CF}_{2\text{D}}$ along the direction (\mathbf{u}') normal to \mathbf{k} to get 1D-CF at each angle using the following formula:

$$\text{CF}_{1\text{D}}(r, \theta_r) = \int_{-\infty}^{+\infty} \text{CF}_{2\text{D}}(r \cos \theta_k - u' \sin \theta_k, r \sin \theta_k + u' \cos \theta_k) du' \quad (3)$$

Secondly, we calculate the Fourier transformation (FT) of the 1D-CF to get the corresponding slice of 2D-PSD at each angle using the following formula:

$$\text{PSD}_{2\text{D}}(k, \theta_k) = \int_{-\infty}^{+\infty} \text{CF}_{1\text{D}}(r, \theta_k) \exp(-ikr) dr \quad (4)$$

Finally, the $\text{PSD}_{2\text{D}}$ is assembled by putting the slices of 2D-PSD at each angle together. The third way is to do the two dimensional Fourier transformation (2D-FT) of $\text{CF}_{2\text{D}}(r_{\parallel}, r_{\perp})$:

$$\text{PSD}_{2\text{D}}(k_{\parallel}, k_{\perp}) = \int_{-\infty}^{+\infty} \int_{-\infty}^{+\infty} \text{CF}_{2\text{D}}(r_{\parallel}, r_{\perp}) \exp(-i(k_{\parallel} r_{\parallel} + k_{\perp} r_{\perp})) dr_{\parallel} dr_{\perp} \quad (5)$$

Here, we set $\sigma_{\parallel 1} = 0.25$, $\sigma_{\perp 1} = 2.0$, $\sigma_{\parallel 2} = 2.0$, and $\sigma_{\perp 2} = 0.25$. The origin $\text{CF}_{2\text{D}}$ and the transferred $\text{PSD}_{2\text{D}}$ obtained by the three methods above are given in Figure 1. From Figure 1, the $\text{PSD}_{2\text{D}}$ obtained by the three different ways are in accordance with each other. This confirms that the the conversion between $\text{CF}_{2\text{D}}$ and $\text{PSD}_{2\text{D}}$ based on the projection-slice theorem is credible.

3. Data analysis and results

Four fast solar wind streams , with their magnetic field measured by the Magnetic Field Investigation (MFI; Lepping et al. (1995)) and particle distribution measured by the Three-Dimensional Plasma Analyser (3DP; Lin et al. (1995)), are investigated at the time cadence of 3s. The time intervals for the four fast solar wind streams are from 12:00 UT 30 January to 00:00 UT 4 February in 1995 (stream 1), from 06:00 UT 17 January to 06:00 UT 20 January in 2007 (stream 2), from 00:00 UT 11 February to 12:00 UT 14 February in 2008 (stream 3), from 12:00 UT 12 July to 12:00 UT 15 July in 2008 (stream 4), respectively. The four streams are typical fast streams, with a speed more than 600 km s^{-1} , a density roughly $2\text{-}4 \text{ cm}^{-3}$, a temperature around 20 eV, and a magnetic field about 4-6 nT.

The transformation from $\text{CF}_{2\text{D}}$ to $\text{PSD}_{2\text{D}}$ based on the projection-slice theorem (He et al., 2013) is applied to \mathbf{B} , \mathbf{V} , $\mathbf{Z}_{\text{major}}$, and $\mathbf{Z}_{\text{minor}}$ to calculate $\text{PSD}_{2\text{D},\mathbf{B}}$, $\text{PSD}_{2\text{D},\mathbf{V}}$, $\text{PSD}_{2\text{D},\mathbf{Z}_{\text{major}}}$, and $\text{PSD}_{2\text{D},\mathbf{Z}_{\text{minor}}}$, respectively. This method yields the relative normalized values ($\text{PSD}_{2\text{D},\text{relative}}$). To get the absolute values, we use the following formula:

$$\text{PSD}_{2\text{D},\text{absolute}}(k, \theta_k) = \text{PSD}_{2\text{D},\text{relative}}(k, \theta_k) \cdot \frac{\text{Power}_{\text{absolute}}}{\text{Power}_{\text{relative}}} \quad (6)$$

with $\text{Power}_{\text{absolute}} = \int_{f_0}^{f_1} \text{PSD}_{\text{FFT}} df$ and $\text{Power}_{\text{relative}} = \int_{f_0}^{f_1} \int_0^{2\pi} \text{PSD}_{2\text{D},\text{relative}} \cdot f df d\theta$. f_0 and f_1 stand for the lower and upper limit of the frequency range used to calculate the power, respectively. Here, f_0 and f_1 are set to 10^{-4} and 0.067 Hz. PSD_{FFT} is obtained by the Fast Fourier transformation of the whole time sequence. Then the residual energy $E_{\text{R}} = \text{PSD}_{2\text{D},\text{absolute},\mathbf{V}} - \text{PSD}_{2\text{D},\text{absolute},\mathbf{B}}$, Alfvén ratio $R_{\text{A}} = \frac{\text{PSD}_{2\text{D},\text{absolute},\mathbf{V}}}{\text{PSD}_{2\text{D},\text{absolute},\mathbf{B}}}$ and Elsässer ratio $R_{\text{E}} = \frac{\text{PSD}_{2\text{D},\text{absolute},\mathbf{Z}_{\text{minor}}}}{\text{PSD}_{2\text{D},\text{absolute},\mathbf{Z}_{\text{major}}}}$ in wave-vector space are investigated consequently.

Figure 2 displays the spectra $\text{PSD}_{2\text{D}}$ of magnetic field \mathbf{B} (upper panels) and velocity \mathbf{V} (lower panels) for the four fast streams. The spectra $\text{PSD}_{2\text{D}}$ of magnetic field \mathbf{B} behave similar to that obtained by He et al. (2013). The spectra $\text{PSD}_{2\text{D}}$ of \mathbf{B} for the four fast streams show a similar anisotropic distribution in wave-vector space. The PSD is distributed mainly along a ridge which is inclined toward the k_{\perp} axis. Besides the similarity, the distribution of the spectra $\text{PSD}_{2\text{D}}$ also shows some difference between different streams. For example, stream 1 and stream 2 show a component which is aligned with the k_{\perp} axis. We are not currently sure whether the difference between different streams is caused by some underlying physical difference or by the method uncertainty or by both. In the future, more effort is needed to be done to quantitatively estimate the method uncertainty and distinguish it from the physical signal. The spectra $\text{PSD}_{2\text{D}}$ of velocity \mathbf{V} show a similar anisotropy pattern as that of magnetic field \mathbf{B} , suggesting the signature of oblique Alfvén waves.

To investigate the spectral anisotropy of Elsässer variables, the Elsässer spectra in wave-vector space are obtained and shown in Figure 3. The spectra $\text{PSD}_{2\text{D}}$ of $\mathbf{Z}_{\text{major}}$ and $\mathbf{Z}_{\text{minor}}$ both show anisotropy in the wave-vector space. However, the anisotropy pattern is different for $\mathbf{Z}_{\text{major}}$ and $\mathbf{Z}_{\text{minor}}$. The spectra $\text{PSD}_{2\text{D}}$ of $\mathbf{Z}_{\text{major}}$ share a similar anisotropic pattern with that of magnetic field \mathbf{B} , and velocity \mathbf{V} , while the spectra $\text{PSD}_{2\text{D}}$ of $\mathbf{Z}_{\text{minor}}$ show a very different anisotropy with the main features of $\text{PSD}_{2\text{D}}$ distributed along the k_{\perp} axis. The spectra $\text{PSD}_{2\text{D}}$ of $\mathbf{Z}_{\text{minor}}$ normalized to the $\text{PSD}_{2\text{D}}$ with the same k_{\perp} but with $k_{\parallel} = 0$ (upper panels in Figure 4) reveal further evidence that the spectra $\text{PSD}_{2\text{D}}$ of $\mathbf{Z}_{\text{minor}}$ is mainly distributed at small k_{\parallel} . These results suggest that the anisotropy of the subdominant mode $\mathbf{Z}_{\text{minor}}$ is stronger than that of the dominant mode $\mathbf{Z}_{\text{major}}$, which is consistent with the observational result based on the reduced spectrum (Wicks et al., 2011) and the simulation result (Cho & Lazarian, 2014).

The residual energy E_{R} for all the four fast streams is less than 0, meaning that the magnetic energy is dominant over kinetic energy. The residual energy E_{R} is normalized to k_{\perp} axis, using the formula $E_{\text{R},\text{norm}} = \frac{E_{\text{R}}(k_{\parallel}, k_{\perp})}{E_{\text{R}}(k_{\parallel}=0, k_{\perp})}$, and shown in the lower panels in Figure 4. As seen from the

normalized residual energy $E_{R,\text{norm}}$, the residual energy E_R is concentrated at small k_{\parallel} . This result gives the clear observational support to the simulation results of Boldyrev & Perez (2009) and Wang et al. (2011), which showed a condensate of magnetic energy during cascading of Alfvén waves due to the breakdown of the mirror symmetry in nonbalanced turbulence.

The distribution of R_A (upper panels in Figure 5) and R_E (lower panels in Figure 5) both show anisotropy. Close to the k_{\perp} axis, R_A becomes smaller, suggesting that the dominance of magnetic energy over the kinetic energy becomes significant at small k_{\parallel} . R_E close to the k_{\perp} axis is much larger than at other angles, suggesting that the difference between the energy of $\mathbf{Z}_{\text{major}}$ and that of $\mathbf{Z}_{\text{minor}}$ is larger close to the k_{\perp} axis.

4. Summary and discussions

In this paper, we first did a benchmark test of the conversion between $\text{CF}_{2\text{D}}$ and $\text{PSD}_{2\text{D}}$, confirming that the conversion obtained directly from the corresponding formula, by the transformation based on the projection-slice theorem, and by the transformation based on two dimensional inverse Fourier are in accordance with each other. This experiment manifests the applicability of the transformation based on the projection-slice theorem to estimate $\text{PSD}_{2\text{D}}$.

Based on the transformation, we investigated the spectral anisotropy of Elsässer variables in 2D wave-vector space for the first time. We also studied the distribution of residual energy E_R , Alfvén ratio R_A and Elsässer ratio R_E , which have not been studied in the $(k_{\parallel}, k_{\perp})$ space before. Four fast streams observed by the WIND spacecraft were studied in this work.

The spectra $\text{PSD}_{2\text{D}}$ of $\mathbf{Z}_{\text{major}}$ and $\mathbf{Z}_{\text{minor}}$ both show anisotropy in the wave-vector space. However, the anisotropic pattern of $\mathbf{Z}_{\text{major}}$ and $\mathbf{Z}_{\text{minor}}$ is different and the anisotropy of $\mathbf{Z}_{\text{minor}}$ seems stronger than that of $\mathbf{Z}_{\text{major}}$, which is consistent with the observational result from the reduced spectrum (Wicks et al., 2011) and the simulation result (Cho & Lazarian, 2014).

For each of the four fast streams, the spectra $\text{PSD}_{2\text{D}}$ of \mathbf{B} , \mathbf{V} , and $\mathbf{Z}_{\text{major}}$ share a similar anisotropic pattern as that obtained by He et al. (2013). The spectra $\text{PSD}_{2\text{D}}$ is distributed mainly along a ridge which is inclined toward the k_{\perp} axis. This suggests that $\mathbf{Z}_{\text{major}}$ probably correspond to the oblique Alfvénic fluctuations propagating outwardly.

Differently from that of \mathbf{B} , \mathbf{V} , and $\mathbf{Z}_{\text{major}}$, the spectra $\text{PSD}_{2\text{D}}$ of $\mathbf{Z}_{\text{minor}}$ is distributed mainly along the k_{\perp} axis. The Elsässer ratio R_E is larger at large θ_{kB} angles than at other angles, suggesting that the difference between the spectra $\text{PSD}_{2\text{D}}$ of $\mathbf{Z}_{\text{major}}$ and that of $\mathbf{Z}_{\text{minor}}$ becomes more evident when it is getting close to the k_{\perp} axis. The spectra $\text{PSD}_{2\text{D}}$ of $\mathbf{Z}_{\text{minor}}$ normalized to the $\text{PSD}_{2\text{D}}$ with the same k_{\perp} but with $k_{\parallel} = 0$ further demonstrates that the power of $\mathbf{Z}_{\text{minor}}$ is concentrated at small k_{\parallel} . The Alfvén ratio R_A close to the k_{\perp} axis is much smaller compared to that at other angles. If the plasma is thermally anisotropic and component-drifted, the Alfvén ratio will be very low, even when $\mathbf{Z}_{\text{minor}}$ stands for the inward propagating Alfvén wave. So, the presence of inward

propagating Alfvén waves can not be excluded. If the cascade of $\mathbf{Z}_{\text{minor}}$ is driven by $\mathbf{Z}_{\text{major}}$, this may suggest that the cascade is anisotropic and probably mainly along the k_{\perp} direction. The magnetic structure without velocity fluctuations and the non-Alfvénic fluctuation with $k_{\parallel} = 0$ both could lead to the power concentration of $\mathbf{Z}_{\text{minor}}$ and the low Alfvén ratio. Further work is required in the future to understand what $\mathbf{Z}_{\text{minor}}$ mostly represents.

Though the spectra of \mathbf{B} and \mathbf{V} share a similar spectral anisotropic pattern, there are still differences between them as revealed by the anisotropic distribution of E_R and R_A . Close to the k_{\perp} axis, R_A becomes smaller and $|E_R|$ becomes larger, suggesting that the dominance of the magnetic energy over the kinetic energy becomes significant. The residual energy condensate at small k_{\parallel} confirms observationally the findings in the simulation results of Boldyrev & Perez (2009) and Wang et al. (2011).

It should be noted that, $\mathbf{Z}_{\text{minor}}$ may be anti-correlated with $\mathbf{Z}_{\text{major}}$ due to the dominance of magnetic energy over kinetic energy. The unequipartition between magnetic and kinetic energy may be the case for Alfvén waves with kinetic effects if the plasma is thermally anisotropic and component-drifted. We have tried to re-estimate the spectra PSD_{2D} of $\mathbf{Z}_{\text{major}}$ and $\mathbf{Z}_{\text{minor}}$ after correcting for kinetic effects from the thermal anisotropy. The recalculated distribution of PSD_{2D} of $\mathbf{Z}_{\text{major}}$ remain almost unchanged. However, the PSD_{2D} of $\mathbf{Z}_{\text{minor}}$ after correcting the thermal anisotropy can not be reconstructed with good quality, which might be due to the possible over-correction of the thermal anisotropy on the weak signal of $\mathbf{Z}_{\text{minor}}$.

In the critical balance theory of Goldreich & Sridhar (1995), the eddies are filament shaped. In simulations the eddies usually have a ribbon shape (Müller & Biskamp, 2000; Biskamp & Müller, 2000; Maron & Goldreich, 2001) rather than a filament. Boldyrev (2006) extended critical balance theory to account for this 3D anisotropy. Chen et al. (2013) investigated the local three dimensional structure functions of the inertial range plasma turbulence based on observation for the first time. They found that the Alfvénic fluctuations are three-dimensionally anisotropic dependent on the scales. In future, we intend to extend this method to three dimension to investigate the PSD in 3D wave-vector space and compare the result with former theoretical and simulation results. To promote the usage of the method in the community, further calibration of this method, e.g. to compare the reconstructed PSD with the known PSD, the turbulent fluctuations of which is measured for the reconstruction (Horaites et al., 2015), is required (Oughton et al., 2015) (private communication with Tulasi Parashar).

The group from Peking University was supported by NSFC under 41174148, 41222032, 41231069, 41421003, 41474147, 41274172, and 41474148. J.S.H., C.Y.T., C.H.K.C., X.W., and R.W. are also members of the ISSI/ISSI-BJ international team 304.

REFERENCES

- Bavassano, B., Pietropaolo, E., & Bruno, R. 1998, *J. Geophys. Res.*, 103, 6521
- Belcher, J. W., & Davis, Jr., L. 1971, *J. Geophys. Res.*, 76, 3534
- Biskamp, D., & Müller, W.-C. 2000, *Physics of Plasmas*, 7, 4889
- Boldyrev, S. 2006, *Physical Review Letters*, 96, 115002
- Boldyrev, S., & Perez, J. C. 2009, *Physical Review Letters*, 103, 225001
- Boldyrev, S., Perez, J. C., & Zhdankin, V. 2012, in *American Institute of Physics Conference Series*, Vol. 1436, *American Institute of Physics Conference Series*, ed. J. Heerikhuisen, G. Li, N. Pogorelov, & G. Zank, 18–23
- Bruno, R., Bavassano, B., & Pietropaolo, E. 1996, in *American Institute of Physics Conference Series*, Vol. 382, *American Institute of Physics Conference Series*, ed. D. Winterhalter, J. T. Gosling, S. R. Habbal, W. S. Kurth, & M. Neugebauer, 229–232
- Chen, C. H. K., Bale, S. D., Salem, C. S., & Maruca, B. A. 2013, *ApJ*, 770, 125
- Chen, C. H. K., Horbury, T. S., Schekochihin, A. A., et al. 2010, *Physical Review Letters*, 104, 255002
- Chen, C. H. K., Mallet, A., Yousef, T. A., Schekochihin, A. A., & Horbury, T. S. 2011, *MNRAS*, 415, 3219
- Cho, J., & Lazarian, A. 2014, *ApJ*, 780, 30
- Galtier, S., Nazarenko, S. V., Newell, A. C., & Pouquet, A. 2000, *Journal of Plasma Physics*, 63, 447
- Gogoberidze, G., Chapman, S. C., & Hnat, B. 2012, *Physics of Plasmas*, 19, 102310
- Goldreich, P., & Sridhar, S. 1995, *ApJ*, 438, 763
- Grappin, R., Leorat, J., & Pouquet, A. 1983, *A&A*, 126, 51
- He, J., Tu, C., Marsch, E., Bourouaine, S., & Pei, Z. 2013, *ApJ*, 773, 72
- Horaites, K., Boldyrev, S., Krasheninnikov, S. I., et al. 2015, *Physical Review Letters*, 114, 245003
- Horbury, T. S., Forman, M., & Oughton, S. 2008, *Physical Review Letters*, 101, 175005
- Horbury, T. S., Wicks, R. T., & Chen, C. H. K. 2012, *Space Sci. Rev.*, 172, 325
- Howes, G. G., & Nielson, K. D. 2013, *Physics of Plasmas*, 20, 072302

- Lepping, R. P., Acuña, M. H., Burlaga, L. F., et al. 1995, *Space Sci. Rev.*, 71, 207
- Lin, R. P., Anderson, K. A., Ashford, S., et al. 1995, *Space Sci. Rev.*, 71, 125
- Lithwick, Y., & Goldreich, P. 2003, *ApJ*, 582, 1220
- Lithwick, Y., Goldreich, P., & Sridhar, S. 2007, *ApJ*, 655, 269
- Luo, Q. Y., & Wu, D. J. 2010, *ApJ*, 714, L138
- Maron, J., & Goldreich, P. 2001, *ApJ*, 554, 1175
- Matthaeus, W. H., & Goldstein, M. L. 1982, *J. Geophys. Res.*, 87, 6011
- Müller, W.-C., & Biskamp, D. 2000, *Physical Review Letters*, 84, 475
- Müller, W.-C., & Grappin, R. 2005, *Physical Review Letters*, 95, 114502
- Narita, Y., Glassmeier, K.-H., Sahraoui, F., & Goldstein, M. L. 2010, *Physical Review Letters*, 104, 171101
- Nielson, K. D., Howes, G. G., & Dorland, W. 2013, *Physics of Plasmas*, 20, 072303
- Oughton, S., Matthaeus, W. H., Wan, M., & Osman, K. T. 2015, *Royal Society of London Philosophical Transactions Series A*, 373, 40152
- Perez, J. C., & Boldyrev, S. 2009, *Physical Review Letters*, 102, 025003
- Podesta, J. J. 2009, *ApJ*, 698, 986
- Roberts, D. A., Klein, L. W., Goldstein, M. L., & Matthaeus, W. H. 1987, *J. Geophys. Res.*, 92, 11021
- Sahraoui, F., Goldstein, M. L., Belmont, G., Canu, P., & Rezeau, L. 2010, *Physical Review Letters*, 105, 131101
- Shebalin, J. V., Matthaeus, W. H., & Montgomery, D. 1983, *Journal of Plasma Physics*, 29, 525
- Tu, C. Y., & Marsch, E. 1992, in *Solar Wind Seven Colloquium*, ed. E. Marsch & R. Schwenn, 549–554
- Tu, C.-Y., & Marsch, E. 1993, *J. Geophys. Res.*, 98, 1257
- Wang, X., Tu, C., He, J., Marsch, E., & Wang, L. 2014, *ApJ*, 783, L9
- Wang, Y., Boldyrev, S., & Perez, J. C. 2011, *ApJ*, 740, L36
- Wicks, R. T., Horbury, T. S., Chen, C. H. K., & Schekochihin, A. A. 2011, *Physical Review Letters*, 106, 045001

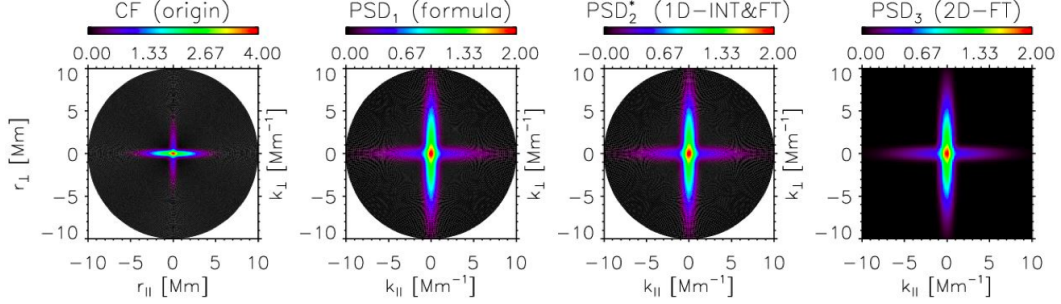


Fig. 1.— Benchmark test of the conversion from CF_{2D} to PSD_{2D} . From left to right: the original CF_{2D} , PSD_{2D} calculated from Equation 2, PSD_{2D} obtained from the transformation based on the projection theorem which involves 1D-INT and FT, and PSD_{2D} obtained by 2D-FT.

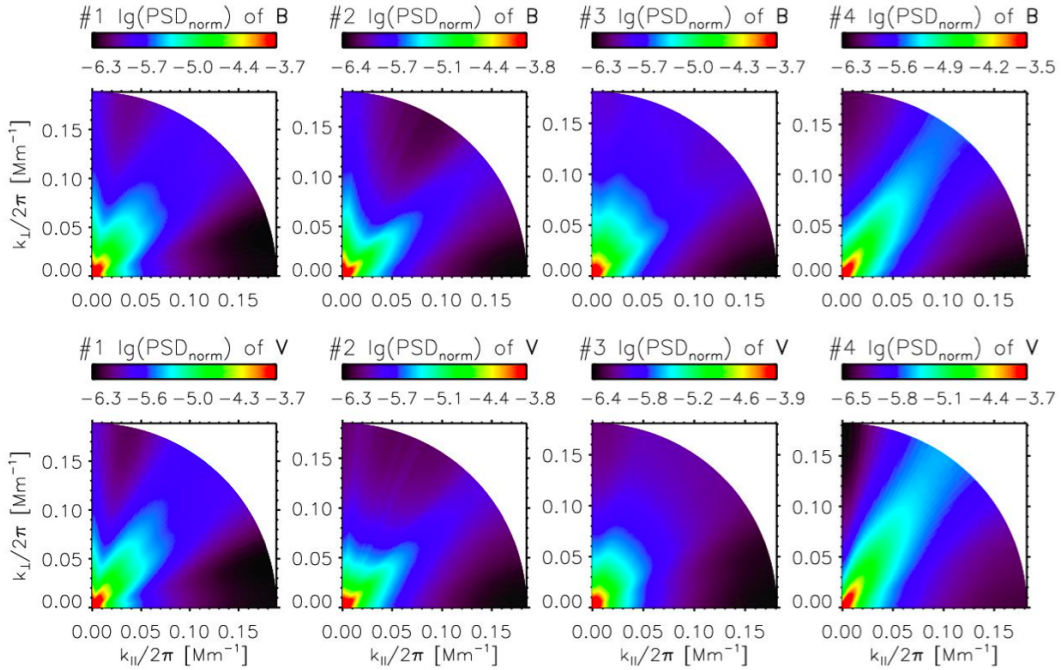


Fig. 2.— The spectra PSD_{2D} of \mathbf{B} (upper panels) and \mathbf{V} (lower panels), which are normalized to the maximum value, for the four fast solar wind streams.

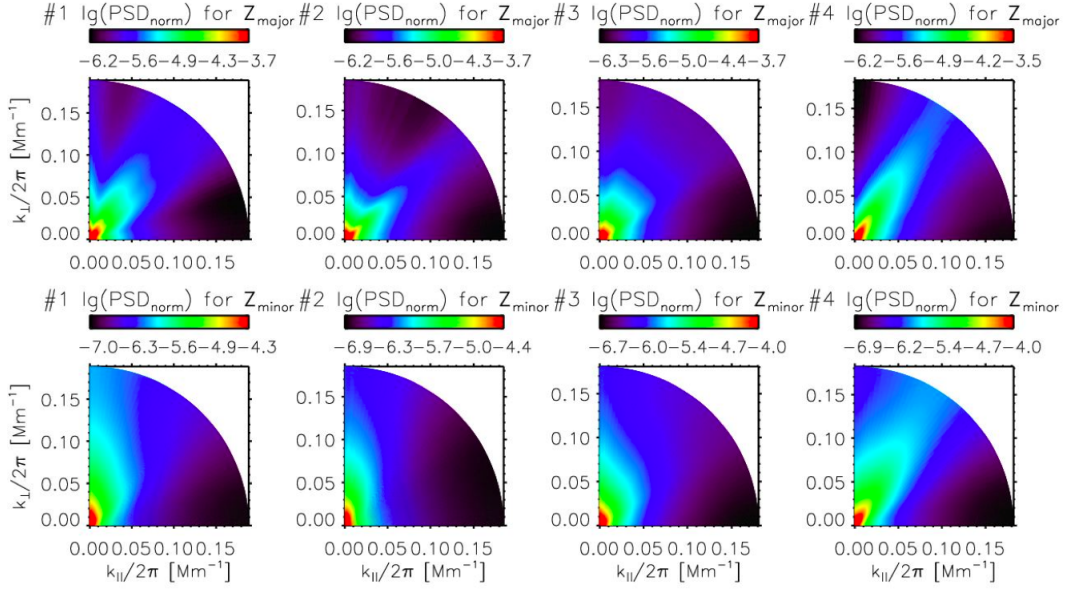


Fig. 3.— The spectra $\text{PSD}_{2\text{D}}$ of $\mathbf{Z}_{\text{major}}$ (upper panels) and $\mathbf{Z}_{\text{minor}}$ (lower panels), which are normalized to the maximum value, for the four fast solar wind streams.

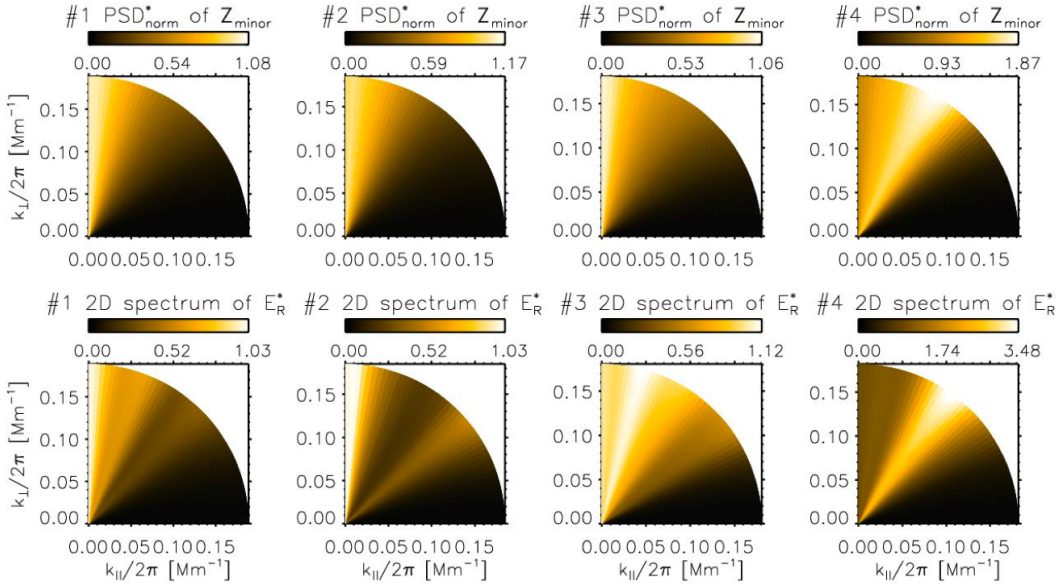


Fig. 4.— The normalized spectra of $\mathbf{Z}_{\text{minor}}$ ($\frac{\mathbf{Z}_{\text{minor}}(k_{\parallel}, k_{\perp})}{\mathbf{Z}_{\text{minor}}(k_{\parallel}=0, k_{\perp})}$; upper panels) and residual energy ($\frac{E_{\text{R}}(k_{\parallel}, k_{\perp})}{E_{\text{R}}(k_{\parallel}=0, k_{\perp})}$; lower panels), for the four fast solar wind streams.

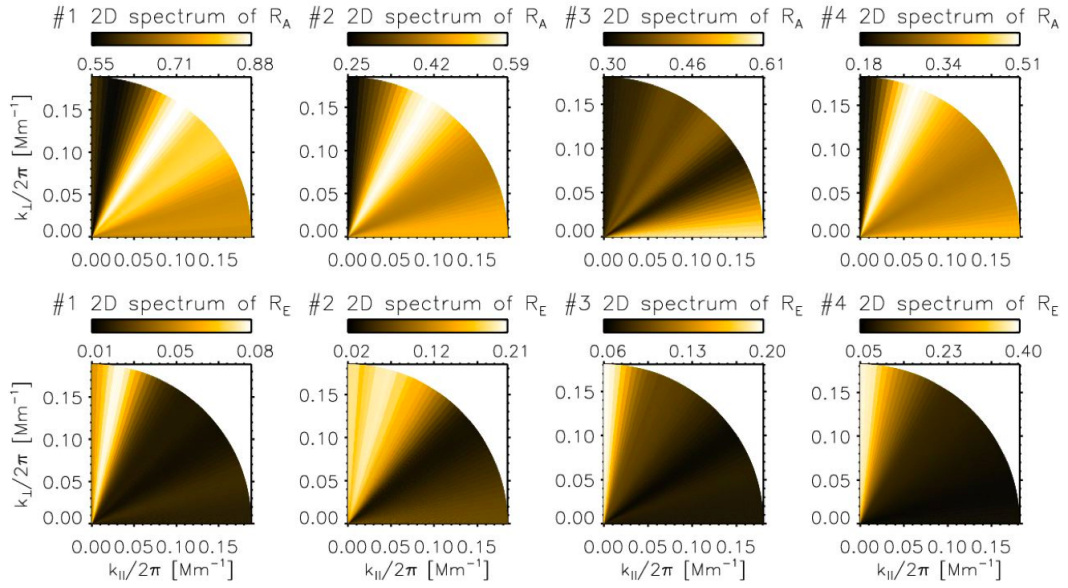


Fig. 5.— The wave-vector distribution of Alfvén ratio R_A (upper panels) and Elsässer ratio R_E (lower panels) for the four fast solar wind streams.